Quest Journals
Journal of Architecture and Civil Engineering
Volume 9 ~ Issue 7 (2024) pp: 21-33
ISSN(Online) : 2321-8193
www.questjournals.org

Research Paper

Estimating Vegetation Biomass and Cover Across Large Plots in Edo Forest Reserve and Grass grass-dominated drylands Using Terrestrial Lidar and Machine Learning

Michael Obeten[1], Suleiman Ibrahim Abubakar[2], Ahmed Jimoh[3]
[1,3]*Department of Computer Science, School of Information and Communication Technology, Auchi Polytechnic, Auchi, Edo State, Nigeria*
[2]*Department of Agricultural Engineering, School of Engineering Technology, Auchi Polytechnic, Auchi, Edo State, Nigeria*

Abstract
Terrestrial laser scanning (TLS) offered an efficient, precise, and non-destructive approach for inventorying vegetation structure over distances extending up to hundreds of meters. In this study, we proposed a novel methodology integrating TLS with machine learning techniques to model and map canopy cover and biomass across large plots of vegetation. We collected high-definition TLS scans of 26 one-hectare plots situated in desert grasslands and big sagebrush shrublands in southwest Idaho, USA. The Random Forests machine learning algorithm was employed to develop decision tree models predicting biomass and canopy cover for various vegetation classes based on statistical descriptors of the TLS point cloud data. Manual measurements of vegetation characteristics within each plot were utilized for training and validation. Models utilizing five or fewer TLS descriptors effectively predicted the canopy cover fraction of shrubs (R^2 = 0.77, RMSE = 7%), annual grasses (R^2 = 0.70, RMSE = 21%), perennial grasses (R^2 = 0.36, RMSE = 12%), forbs (R^2 = 0.52, RMSE = 6%), bare earth or litter (R^2 = 0.49, RMSE = 19%), and the biomass of shrubs (R^2 = 0.71, RMSE = 175 g) and herbaceous vegetation (R^2 = 0.61, RMSE = 99 g). While our models explained much of the variability between predictions and manual measurements, future applications could enhance accuracy by addressing methodological errors encountered. This study demonstrated that TLS could extend manual vegetation measurement from small to large plots in grasslands and shrublands, with potential applications to similar ecosystems. Our method circumvented the need for individual plant classification, a challenging and time-consuming process in previous TLS-based vegetation inventories. Enhanced TLS application in shrub-steppe ecosystems supported vegetation inventories, environmental modeling, and broader datasets from aerial and spaceborne sensors.

Keywords: *rangelands; carbon; point cloud; lidar; biomass; classification; land cover; remote sensing; machine learning; vegetation type; Structure from Motion (SfM).*

***R**eceived 14 July, 2024; **R**evised 28 July, 2024; **A**ccepted 30 July, 2024*
P**ublished with open access at **www.questjournals.org

I. Introduction

Sagebrush steppe, a biome characterized by shrub and bunchgrass dominance, spans approximately 47 million hectares of semiarid rangelands in the western United States (Bukowski and Baker 2013). However, this ecosystem faces rapid degradation, fragmentation, and loss. The primary driver of this decline is the "grass-fire cycle" (D'Antonio and Vitousek 1992), where frequent wildfires foster the invasion of nonnative grasses and forbs, exacerbating future fire intensity and frequency. This cycle often leads to the replacement of sagebrush ecosystems with a stable state of nonnative pyric grassland (Knick 1999, Balch et al 2013). The shift results in increased wildfire risk, reduced soil retention, diminished forage quality, and lower biodiversity (Brooks et al. 2004, Rowland et al. 2011, Balch et al. 2013, Ripplinger et al. 2015). An urgent example of this threat is the Morley Nelson Snake River Birds of Prey National Conservation Area (NCA) in southwest Idaho, where only about one-third of the 195,000-hectare area remains occupied by native shrub communities due to the impact of recent fires (USDI BLM 2008).

Addressing the conservation and restoration of sagebrush steppe ecosystems is critical (e.g., Pyke et al. 2015). Accurate, scalable, and practical methods for vegetation inventory are essential for habitat monitoring,

wildfire risk assessment, behavior modeling, and vegetation treatment evaluation. Historically, hand-measured metrics such as transect or frame-based measurements of biomass and structure (e.g., cover, density, height) have been employed, remaining the primary data source for sagebrush habitat inventories (e.g., Reiner et al. 2010). These metrics, which indicate productivity and ecological processes, are vital for managing fuel treatments and grazing resources (e.g., Davies and Bates, 2010, Pyke et al., 2014). Although manual sampling provides precise measurements, it is logistically challenging across extensive, remote, and heterogeneous shrubland landscapes.Airborne and spaceborne optical remote sensing methods offer broad datasets useful for classifying dryland vegetation (e.g., Homer et al. 2012), though they often lack the structural information required for estimating aboveground biomass. Airborne laser scanning (ALS) has been developed for sensing dryland vegetation structure (e.g., Streutker and Glenn 2006, Mitchell et al. 2011), but struggles to accurately capture low biomass herbaceous plants (e.g., Glenn et al. 2016, Li et al. 2017).

Terrestrial laser scanning (TLS) provides a data source that bridges the gap between precise, localized manual measurements and broader, coarser data from aerial and satellite platforms. TLS, typically involving a rotating scanner mounted on an elevated platform, rapidly collects high-density point clouds representing the 3-D positions of surfaces and objects, including herbaceous vegetation. TLS measurements exhibit negligible instrumentation error and can achieve high-resolution collections at ranges up to hundreds of meters with minimal logistical expense (Shan and Toth, 2008, Vosselman and Maas, 2010). However, TLS can be hindered by occlusion, where objects behind other objects are not sampled (Cifuentes et al., 2014). To address this, multiple scans from different positions can be combined (e.g., Cooper et al., 2017, Van der Zande 2008, Wilkes et al., 2017), or the instrument can be elevated to minimize shadowing (Vierling et al. 2013). TLS may also encounter minor irregularities in point cloud density and positional precision due to varying ranges and beam diameters (Telling et al., 2017).

TLS has been successfully applied to measure various forest metrics, including tree stem count, basal area, biomass, height, and canopy gap fraction (Henning and Radtke 2006, Yao et al. 2011, Zhao et al. 2011, Zhao et al. 2012, Calders et al. 2014, Richardson 2014). In shrubland environments, TLS has been used to study individual plants and plot-wide vegetation metrics, including shrub structure, biomass, fuelbed volume, and vegetation density profiles (e.g., Adams 2014, Olsoy et al. 2014b, Loudermilk et al. 2009, Rowell et al., 2016, Vierling et al. 2013).Machine learning algorithms have increasingly been used to classify vegetation and model structural traits from ALS data (e.g., Li et al. 2017), often outperforming simple regression methods. Random Forests, for example, aggregates multiple decision trees to produce robust predictive models with out-of-bag error measures (Breiman 1996, 2001a).

This study demonstrates a workflow utilizing TLS and machine learning (Random Forests) to predict biomass and canopy cover of sagebrush-steppe plants across large plots. The primary objective is to develop a straightforward method for quantifying biomass and cover in sagebrush-steppe ecosystems without requiring individual plant classification. Our models, applied to both existing and new 1-ha plots, exhibit strong predictive power despite some limitations in TLS data and known errors. This approach proves to be efficient, scalable, and resilient for modeling vegetation traits across extensive areas.

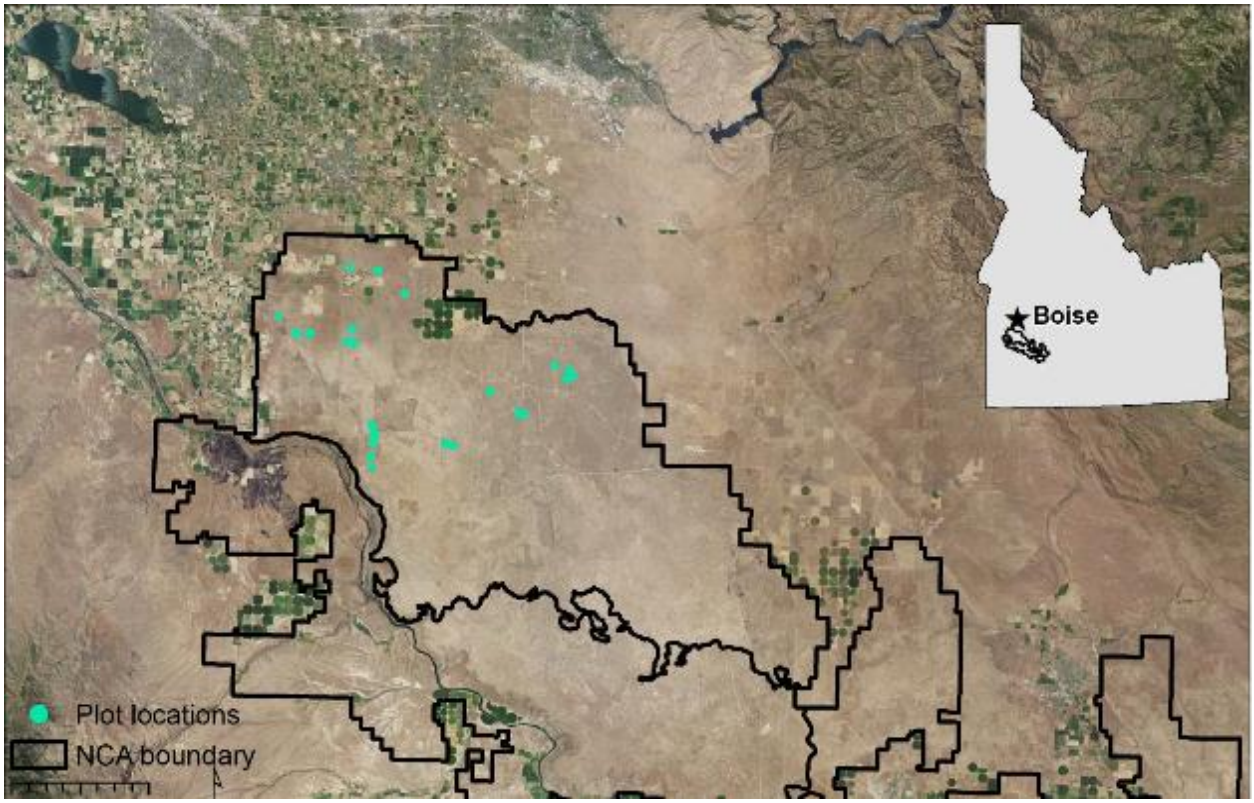

Figure 1*. Location of the NCA study area and plots with manual and TLS vegetation sampling in Edo Forest Reserve, Edo State, Nigeria. The background image is a National Agriculture Imagery Program (NAIP) true-color image.*

2.2 Data Collection

Our workflow for data collection and processing is detailed in Fig. 2 and described below. We performed all TLS sampling between 15 May and 14 June 2023. By this date, grasses and forbs were mostly senescent but structurally intact. We used a stratified random sampling approach to locate twenty-six 1-ha plots, measuring 100 m by 100 m, for manual and TLS vegetation sampling throughout the Edo Forest Reserve, Edo State, Nigeria. The sites spanned a gradient of plant community compositions, including intact forested areas, degraded regions with non-native grasses, and reforested sites containing taller perennial species. The plots were split evenly among sites dominated by shrubs and grasses (n=13 each). In each 1-ha plot, vegetation characteristics were collected manually in nine 1-m² quadrats spaced 25 m apart in a 3 by 3 grid centered on the plot (Fig. 3 and 4). This resulted in a total of 234 1-m² quadrats across 26 plots where paired manual and TLS sampling was performed.

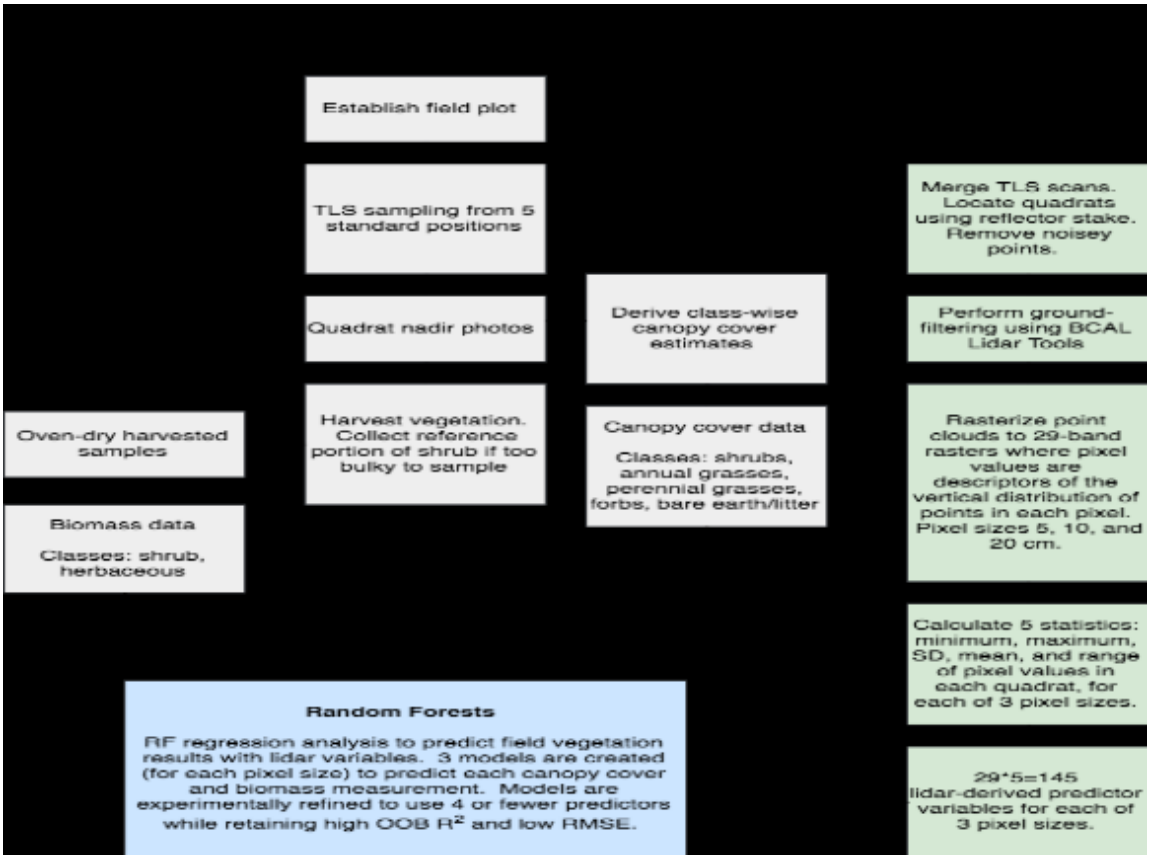

Figure 2. Workflow of data collection, data processing, and Random Forests analysis resulting in predictive models for each cover and biomass class.

We deployed elevated disc reflectors at each plot corner to provide control points for co-registration and geo-registration of TLS scans. A small reflector on a tall stake was placed at the center point of each quadrat to precisely mark its location in the TLS point cloud (after TLS collection, the stake was replaced by a surveyor's flag to mark the center point for manual vegetation sampling). The sides of square 1-m² quadrats were aligned with cardinal directions. We performed the TLS collection using a Riegl VZ-1000 near-infrared (1550 nm) scanner mounted on a 2-m tripod. At a range of 100 m, this instrument has a reported standard deviation of error of 8 mm and a beam diameter of 30 mm (corresponding to a beam divergence of 0.3 mrad) (Riegl, Austria). Single-return scans were performed with 0.02° of separation between pulses. Plots were scanned from five positions, once from the approximate midpoint of each side (using 180° scans) and once from the approximate plot center (using 360° scans). Our experimental setup took approximately 1-2 hours to collect five scans at each 1-ha plot. Slight leeway in scanner location allowed for adaptation to reduce occlusion in each scan (Fig. 3). After scanning was complete, the quadrat stake reflectors were replaced with surveyor's flags.

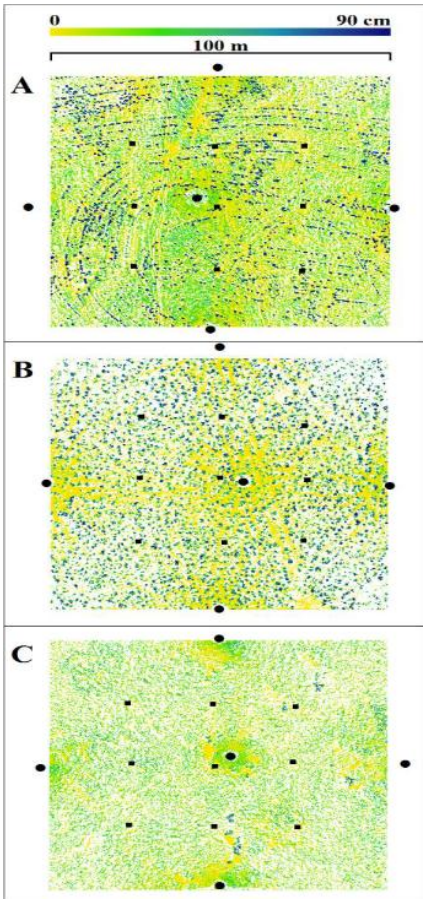

Figure 3. Examples of 1-ha plot layout and TLS-derived data. Black circles show scanning positions while black squares show locations of 1-m² manual sampling quadrats (enlarged for visibility). Coloring shows the maximum aboveground height of TLS points in 5-cm pixels in plots which are seeded with bunchgrasses (A), shrub-dominated (B), and native and non-native annual grass-dominated (C). Pixels occluded from sampling appear as white.

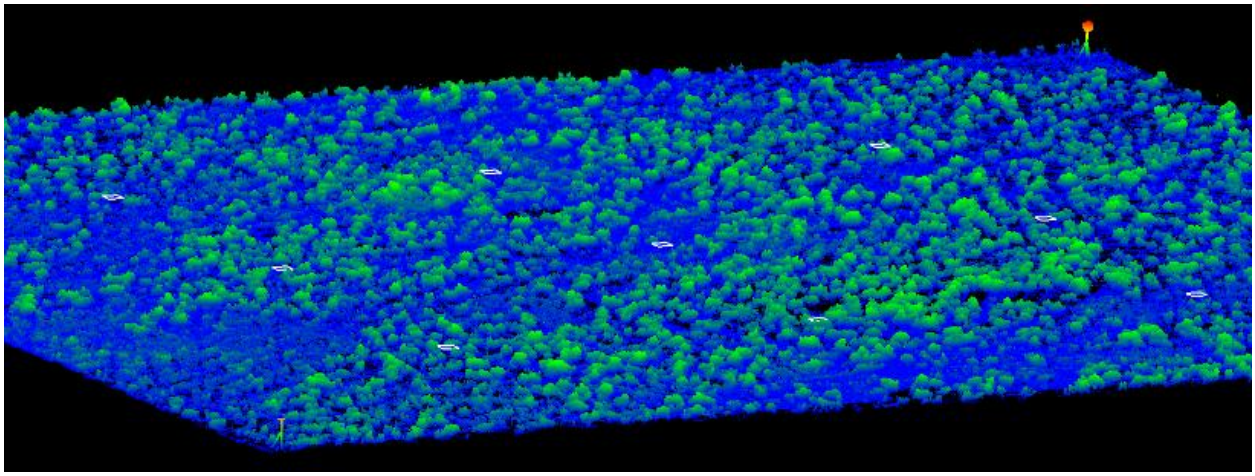

Figure 4. An example of a shrub-dominated plot in the Edo Forest Reserve, Edo State, Nigeria, with quadrats. White lines and numbers indicate the location and layout of the 1-m² quadrats. Elevated disc reflectors are shown at each corner for georegistration. Quadrat 2 was omitted from the analysis due to occlusion (n=136 lidar returns).

2.2 Data Collection

Our workflow for data collection and processing is detailed in Fig. 2 and described below. We conducted all TLS sampling from 15 May to 14 June 2013, a period when grasses and forbs in Edo State were mostly senescent but structurally intact. We employed a stratified random sampling approach to select twenty-

six 1-ha plots, each measuring 100 m by 100 m, for manual and TLS vegetation sampling across various habitats in Edo State. These plots encompassed a range of plant community compositions, including intact shrublands, areas dominated by non-native grasses, and seeded sites with taller perennial bunchgrass species. The plots were evenly divided between shrub-dominated and grass-dominated sites (n=13 each). In each 1-ha plot, vegetation characteristics were manually recorded in nine 1-m² quadrats spaced 25 m apart in a 3 by 3 grid centered on the plot (Fig. 3 and 4). This resulted in a total of 234 1-m² quadrats across 26 plots where paired manual and TLS sampling were performed.

We deployed elevated disc reflectors at each plot corner to provide control points for coregistration and georegistration of TLS scans. A small reflector on a tall stake was placed at the center of each quadrat to precisely mark its location in the TLS point cloud (after TLS collection, the stake was replaced by a surveyor's flag for manual vegetation sampling). The sides of square 1-m² quadrats were aligned with cardinal directions. TLS collection was performed using a Riegl VZ-1000 near-infrared (1550 nm) scanner mounted on a 2-m tripod. At a range of 100 m, this instrument has a reported standard deviation of error of 8 mm and a beam diameter of 30 mm (corresponding to a beam divergence of 0.3 mrad) (Riegl, Austria). Single-return scans were performed with 0.02° of separation between pulses. Plots were scanned from five positions: once from the approximate midpoint of each side (using 180° scans) and once from the approximate plot center (using 360° scans). Our experimental setup took approximately 1-2 hours to collect five scans at each 1-ha plot. Slight leeway in scanner location allowed for adaptation to reduce occlusion in each scan (Fig. 3). After scanning, quadrat stake reflectors were replaced with surveyor's flags.

2.3 Processing

We subsampled the TLS point clouds representing the quadrats to a minimum spacing of 1 cm between points using an octree filter. Points representing quadrat marker reflectors and other spurious ("noise") points were manually removed. Using the BCAL Lidar Tools software (http://bcal.boisestate.edu/tools/lidar), ground filtering (classification of points as ground or vegetation) was performed using an iterative grid-based filtering approach widely applied in similar ecosystems (e.g., Streutker and Glenn 2006). The software was then used to calculate 29 statistical descriptors of the vertical distribution of aboveground TLS points (Table 1), storing this information in 29-band raster files. The BCAL Lidar Tools exploit the rich information about height distributions in 3D point clouds by creating point statistics directly from the point cloud and reporting them in a 2D pixel representation. Each point cloud was used to create three 29-band rasters, each with a different pixel size (5, 10, and 20 cm) to calculate descriptors of point distribution. Considering only pixels containing TLS points, we calculated the minimum, maximum, mean, range, and standard deviation of each of the 29 descriptors listed in Table 1 for each quadrat. As an example, the minimum, maximum, mean, range, and standard deviation of the 50th percentile of all height points within each pixel were calculated at the quadrat level. Calculating five statistics about each of 29 descriptors yielded a total of 145 statistics about point cloud distributions in each quadrat. Hereafter, these 145 statistics are referred to as predictors.

2.4 Quadrat Quality Control

Through the data review process, we identified 28 quadrats as unfit for inclusion in our analysis. Twenty-two of these were discarded due to errors in quadrat placement resulting from miscommunication between TLS and manual field sampling teams. One quadrat was discarded due to a rare ground filtering error identified during a cursory inspection of the classified TLS point cloud. Additionally, we set a minimum threshold of 150 TLS returns (after subsampling to 1-cm spacing) to include a quadrat in the modeling. This threshold was set to exclude quadrats where occlusion prevented the collection of meaningful structural data (see Fig. 4 for an example). Five quadrats were discarded using this criterion. After removing these 28 quadrats, the remaining 206 were used for further analysis.

Table 1. Descriptors calculated from the TLS point cloud distribution within each pixel. The minimum, maximum, mean, range, and standard deviation of each of the descriptors (n=29) within the bounds of each quadrat were used as predictor variables. All points with a modeled height greater than 0 were classified as vegetation.

Descriptor	Description
Minimum height	The lowest height value recorded in the point cloud for each pixel.
5th percentile height	The height value below which 5% of the point cloud heights fall.
10th percentile height	The height value below which 10% of the point cloud heights fall.
25th percentile height	The height value below which 25% of the point cloud heights fall.
50th percentile height	The median height value, where 50% of the point cloud heights are below and 50% are above.
75th percentile height	The height value below which 75% of the point cloud heights fall.
90th percentile height	The height value below which 90% of the point cloud heights fall.

95th percentile height	The height value below which 95% of the point cloud heights fall.
Maximum height	The highest height value recorded in the point cloud for each pixel.
Mean height	The average height value of the point cloud for each pixel.
Standard deviation of heights	Measure of the variation or dispersion of heights in the point cloud.
Range of heights	Difference between the maximum and minimum height values in the point cloud.
Interquartile range of heights	The range between the 25th and 75th percentiles of height values.
Kurtosis of heights	Measure of the "tailedness" of the height distribution.
Skewness of heights	Measure of the asymmetry of the height distribution.
Variance of heights	Measure of the spread of height values around the mean.
Coefficient of variation of heights	Ratio of the standard deviation to the mean height, expressed as a percentage.
Mean absolute deviation from mean height (AAD)	Average of the absolute deviations from the mean height.
Median absolute deviation from median height (MAD)	Median of the absolute deviations from the median height, multiplied by 1.4826.
Texture of heights (standard deviation between 5 cm and 15 cm)	Standard deviation of heights within a 5 cm to 15 cm vertical range.
Canopy relief ratio of height points	Ratio calculated as (mean height - min height) / (max height - min height).
Percent of returns modeled as ground	Percentage of point cloud returns classified as ground.
Percent of heights between 0 and 1 m tall	Percentage of point cloud returns with heights between 0 and 1 meter.
Percent of heights between 1 and 2.5 m tall	Percentage of point cloud returns with heights between 1 and 2.5 meters.
Count of vegetation returns	Number of point cloud returns classified as vegetation.
Count of ground returns	Number of point cloud returns classified as ground.
Count of all returns	Total number of point cloud returns.
Ratio of vegetation returns to ground returns	Ratio of the number of vegetation returns to ground returns.
Ratio of vegetation returns to total returns	Ratio of the number of vegetation returns to the total number of returns.

2.5 Random Forests Analysis

We used Random Forests to leverage the detailed structural information collected by TLS, predict diverse vegetation traits using a common method, and apply an automated heuristic approach to analyze datasets complicated by varying scan angles, point densities, and patchy occlusion. RF regression (implemented with Salford Predictive Modeler Software Suite version 7, Salford Systems, San Diego, CA) was used to develop models predicting field-measured canopy cover and biomass of vegetation functional groups using the TLS-derived 145 predictors. In each model, we found that the majority of predictors had low influence, and the inclusion of most actually decreased model performance in the testing datasets. We derived models using an automated forward selection procedure, which creates a 1-predictor model using the strongest solitary predictor, a 2-predictor model by identifying the second predictor which yields the strongest model in combination with the first, and so on. We also tested automated backward selection (iterative removal of the least important predictor) and manual trial-and-error procedures of model derivation, but forward selection discovered superior models in every case. For each of the three sets of predictors created using 5, 10, and 20-cm pixels, we collected the first five models of each vegetation feature produced by forward selection. Among these, we selected the model with the highest R^2 and lowest RMSE that used five or fewer predictors. All R^2 and RMSE values used and reported are out-of-bag.Spatial autocorrelation between field observations was considered, given that the quadrat observations within a plot were close together and could exhibit autocorrelation. We tested for spatial autocorrelation between field observations by taking the residuals from the RF model and running a one-way ANOVA with the 26 plots as the treatments. If autocorrelation was present, the residuals from any plot would tend to be mostly positive or mostly negative. If there was no autocorrelation, the residuals would have random variation around a mean of zero. Using this method, we found no evidence of autocorrelation.

II. Results and Discussion

3.1 Field Canopy Cover and Biomass

The distribution of field-measured biomass and fractional canopy cover were highly non-normal, with most biomass and cover estimates clustering near the low or high ranges of measurements. Likewise, the standard deviation of measurements approached or exceeded the mean measurement of each variable (Table 2). For example, the mean shrub, bare earth/litter, and annual grass cover was 8%, 41%, and 35%, whereas their corresponding standard deviation was 14%, 27%, and 38%, respectively.

Table 2. Statistics describing the manual measurements of cover and biomass (n = 206). Minimum values were all 0. Columns 25th & 75th are percentiles and SD is standard deviation.

Feature	25th	Median	75th	Max	Mean	SD
Shrub cover (%)	0	0	8	61	8	14
Bare earth/litter cover (%)	13	43	61	94	41	27
Annual grass cover (%)	0	13	73	100	35	38
Perennial grass cover (%)	1	7	21	70	13	15
Forb cover (%)	0	0	3	68	4	9
Shrub biomass (g)	0	0	18	2476	106	322
Herbaceous biomass (g)	57	97	180	1193	146	158

3.2 Predicted Canopy Cover and Biomass

Five of seven Random Forest models achieved out-of-bag $R^2 > 0.5$ correlation with manual measurements. Descriptors calculated using a 5-cm pixel size yielded the strongest predictors of forb cover ($R^2 = 0.52$, RMSE = 6%) and herbaceous biomass ($R^2 = 0.61$, RMSE= 99 g) (Tables 3 & 4). A 10-cm pixel size yielded the strongest predictors of shrub cover ($R^2 = 0.77$, RMSE = 7%), annual grass cover ($R^2 = 0.70$, RMSE = 21%), perennial grass cover ($R^2 = 0.36$, RMSE = 12%), bare earth/litter cover ($R^2 = 0.49$, RMSE = 19%), and shrub biomass ($R^2 = 0.71$, RMSE = 175 g) (Tables 3 & 4). A 20-cm pixel size did not yield the strongest predictors of any feature. The precision of our model predictions ranged between 46% and 165% of mean manual measurements (by comparing the lowest RMSE values from Tables 3 & 4 with mean manual measurements in Table 2). For example, the prediction of the bare earth/litter cover class had the lowest RMSE in comparison to the mean of the manual measurements (46%), and the RMSE of the annual grass cover was 60% of the mean manual measurement. These classes were also the dominant cover classes in the field, as measured by mean percent cover data (41% and 35%, respectively, Table 2). In comparison, our model predictions which had high RMSE values (e.g. forb cover and shrub biomass) corresponded to classes that had low vegetation percent cover in our field plots.

We found that while marginal improvements in model quality were made available by testing several pixel sizes for predictor creation, the benefit was unlikely to be great. Despite a sixteen-fold difference in the area of the pixel sizes we tested, in only one case was the difference in strength between the strongest models produced by each pixel size greater than $R^2 = 0.05$ (shrub biomass, difference of $R^2 = 0.13$) (results provided in Supplementary Material). While we did not find a single pixel size for predictor calculation to be consistently superior, predictors from 20-cm pixels never yielded the strongest model, and predictors from 10-cm pixels produced the best across-the-board performance. Given that differences in the models were low, a 10-cm pixel size can be interpreted to be appropriate for predicting vegetation cover and biomass in our study area, representing a compromise between too fine a resolution (5-cm) that over-represents occlusion and too coarse (20-cm) which generalizes subtle differences in the point cloud. Future studies may also wish to test several pixel sizes to discover which yield the most useful predictors of the local environment.

Our use of RF was straightforward. For each vegetation feature, we used a forward selection procedure to derive models using one to five predictors, for each of the 5, 10, and 20-cm pixel predictor sets, and selected the model with the highest R^2 from the fifteen produced. This method is not comprehensive, and it is possible somewhat stronger combinations of predictors exist to model some of our targets. We expect our experience to match the common case where the top several competing models of a single feature exhibit similar strengths (even though the predictors they use may differ), minimizing the importance of which specific model is selected (Breiman 2001b). We presented only models using up to five predictors, although using one or two fewer predictors would generally not cost much predictive strength, and allowing one or two more would not cost much parsimony. The combination of predictors used is inconsistent among models, but some predictors were used more commonly than others (Tables 3 & 4). For example, a statistic describing the 50th percentile (median) of point heights in pixels was the top single predictor in every model, except those of shrub biomass.

Table 3. Predictions of percent canopy cover for annual grass, bare earth/litter, forb, perennial grass, and shrub classes using the optimal pixel size to calculate point statistics, as generated by the first 5 predictor sets yielded by forward stepwise selection. Predictors are listed in the order they were added to the predictor set, and resultant models' predictive strength and root mean square error (RMSE, in %) are also listed. Bolded is the model explaining the most variance and with the lowest RMSE. If N=4 is bolded, then the model used the first four predictors; if N=5 is bolded, then the model used all five predictors. Additional results on the remaining pixel sizes are presented in Supplementary Material.

Vegetation	Pixel size	Predictors	N	R^2	RMSE
Annual grass	10	Mean of 50th percentile heights	1	.59	24
		Standard deviation of maximum heights	2	.62	23
		Mean of ratio of vegetation returns to total returns	3	.67	22
		Mean of ratio of vegetation returns to ground returns	4	.69	21
		Minimum of 50th percentile heights	5	.70	21
Bare earth/litter	10	Maximum of 50th percentile heights	1	.38	21
		Standard deviation of interquartile range of heights	2	.45	20
		Standard deviation of ratio of vegetation returns to ground returns	3	.48	20
		Range of percent of vegetation 0 <&<= 1 m high	4	.48	19
		Mean of percent of vegetation 0 <&<= 1 m high	5	.49	19
Forb	5	Minimum of 50th percentile heights	1	.47	6
		Standard deviation of minimum heights	2	.48	6
		Maximum of 50th percentile heights	3	.51	6
		Mean of canopy relief ratio	4	.52	6
		Mean of 50th percentile heights	5	.51	6
Perennial grass	10	Maximum of 50th percentile heights	1	.19	14
		Minimum of coefficient of variation of heights	2	.27	13
		Maximum of 90th percentile heights	3	.32	13
		Minimum of kurtosis of heights	4	.33	13
		Maximum of interquartile range of heights	5	.36	12
Shrub	10	Maximum of 50th percentile heights	1	.66	8
		Standard deviation of 90th percentile heights	2	.72	7
		Mean of 50th percentile heights	3	.76	7
		Range of skewness of heights	4	.76	7
		Minimum of 50th percentile heights	5	.77	7

Table 4. Predictions of biomass for herbaceous and shrub classes using the optimal pixel size to calculate point statistics, as generated by the first 5 predictor sets yielded by forward stepwise selection. Predictors are listed in the order they were added to the predictor set, and resultant models' predictive strength and root mean square error (RMSE, in grams) are also listed. Bolded is the model explaining the most variance and with the lowest RMSE. Both herbaceous and shrub biomass were best predicted using the first four predictors. Additional results on the remaining pixel sizes are presented in Supplementary Material.

Vegetation	Pixel size	Predictors	N	R^2	RMSE
Herbaceous	5	Mean of 50th percentile heights	1	0.47	115
		Minimum of mean of heights	2	0.57	104
		Mean of count of vegetation returns	3	0.60	100
		Minimum of 50th percentile heights	4	0.61	99
		Maximum of 50th percentile heights	5	0.60	99
Shrub	10	Mean of range of heights	1	0.58	209
		Mean of absolute deviation from mean heights	2	0.68	183
		Mean of standard deviation of heights	3	0.67	185
		Minimum of coefficient of variation of heights	4	0.71	175
		Mean of count of returns	5	0.69	178

3.3 Estimates Without Individual Plant Classification

The class-wise characteristics of vegetation functional groups were predicted without explicit classification and delineation of individual plants or vegetation classes. However, our workflow using pixel statistics to extract information from point clouds yielded models with lower fit to ground truth measurements than those developed using per-plant measures such as crown area or volume (e.g., Vierling et al. 2013, Olsoy et al. 2014a,b, and Greaves et al. 2015). We are unaware of any studies that have attempted to sample large plots (1-ha) in dense shrubland using common oblique scanning from a tripod, and the literature may not represent the difficulty of classifying and delineating small and closely-spaced plants in point clouds where occlusion is pervasive. Automated classification approaches, such as spatial wavelet analysis and eigenvalue separation, have not been demonstrated across point clouds where occlusion is common and the sampled vegetation is small and spatially mixed, as is the common case in TLS collections of desert shrublands. Modeling vegetation characteristics on a per-area, rather than per-plant basis, is especially valuable when complementary manual sampling considers all of the vegetation within (and overhanging) a quadrat, and none of the vegetation extending outside of the quadrat.

There are some disadvantages to avoiding explicit classification in a TLS-based vegetation inventory. The strongest predictive relationships between plant structural indices and traits such as biomass would be expected when a single, complete plant is considered. By contrast, our approach aggregates structural information from predefined grids across 1-m^2 quadrats. This results in measurements that combine information

from all plants and plant classes in a quadrat and excludes portions of plants which extend beyond the quadrat's edge. Aggregating structural data from unclassified plants risks confusing a decision tree when different vegetation compositions of quadrats exhibit similar signals (e.g., the aggregated measurements of points representing several tall and narrow bunchgrasses might resemble the measurements of a single tall and stout shrub). We expect the high RMSE of the shrub biomass predictions were partly caused by these challenges. In fairness, we would expect some misidentification of vegetation to occur in any TLS-based workflow due to structural similarity of certain species in different functional groups (e.g., tall forbs, such as tumble mustards and thistles, resemble shrubs and smaller perennial grasses resemble annual grasses).

3.4 Field Considerations

Our five-position TLS sampling protocol frequently resulted in redundant coverage with excess resolution, but occlusion remained a challenge, particularly in plots with dense shrub cover. In some instances, TLS sampling of vegetation shorter than the top canopies of shrubs was sparse across much of the plot. Despite this, we discarded only 2% of quadrats due to insufficient TLS returns. Partial occlusion was common in the remaining quadrats. Using gridded presence/absence windows, average quadrat sampling coverage of pixels with any number of points was 59% (std = 24%) for a 5-cm grid, 80% (std = 19%) for a 10-cm grid, and 92% (std = 16%) for a 20-cm grid. The success of our models despite occlusion indicates that our methods are effective with practical TLS field collections.Sampling density (returns per m²) varied significantly depending on occlusion and relative position to the scan layout. We analyzed statistics on the counts of TLS returns per quadrat by position (center, middle-edge, corner) and per 1-m² grid cell across grass and shrub-dominated plots. Additionally, we calculated the percentage of quadrats or 1-m² grid cells not meeting the 150-return minimum threshold for modeling. Sites close to scan positions (e.g., center quadrats) typically had thousands more returns compared to those farther away. The distribution of sampling densities across 1-m² quadrats resembled that of 1-m² grid cells, indicating that our quadrat placement protocol adequately represented sampling variability. Only 4% of 1-m² grid cells were below the 150-return minimum threshold. These results confirm that our models are applicable with the reported strength across 1-ha plots (Table 5).

Table 5. Summary of TLS returns and the percentage of quadrats or grid cells below the 150 return minimum threshold for different quadrat positions and vegetation types.

Region Type	Min	25th	Median	75th	Max	Mean	< 150 Returns
Center quadrats (n=1 x 26 plots)	1	474	5,708	8,245	12,600	10,260	0%
Middle-edge quadrats (n=4 x 26)	2	805	1,504	2,782	12,370	1,976	2.9%
Corner quadrats (n=4 x 26)	22	514	930	1,482	6,730	1,213	1.9%
All quadrats (n=9 x 26 plots)	2	666	1,268	2,731	34,770	2,558	2.1%
1-m² grid cells in grass plots (n=10,000 x 13)	0	683	1,216	2,402	70,110	2,534	1.4%
1-m² grid cells in shrub plots (n=10,000 x 13)	0	581	1,312	3,011	103,000	2,936	6.6%
1-m² grid cells in all plots (n=10,000 x 26)	0	639	1,257	2,679	103,000	2,730	4.0%

The primary source of occlusion in TLS sampling was dense shrub canopies, which in plots with the highest shrub cover blocked sampling of nearly half of 5-cm gridded windows within the hectare. On average, the 5 quadrats discarded due to occlusion had relatively high shrub cover (21%), average bare earth/litter cover (41%), and low annual grass cover (5%). This reflects the general composition of shrub-dominated plots and supports our field observation that substantial occlusion within quadrats is largely a consequence of surrounding vegetation rather than low-lying or impenetrable vegetation within the quadrats.

While the ground classification algorithm used has been widely tested in similar shrubland environments (e.g., Glenn et al., 2011; Mitchell et al., 2011; Streutker and Glenn, 2006), errors due to occlusion and confusion between plants and ground surfaces may have contributed to the low R^2 of the model predicting bare earth/litter coverage. Imperfect ground classification and surface modeling can also affect point cloud measurements of height (e.g., Ashcroft et al., 2014; Fan et al., 2014). Improved sampling coverage of 1-ha plots with densely spaced shrubs could be achieved by scanning from more than five positions, moving scan positions inward from the plot edge, or by elevating the TLS further. While classification errors were possible, and we discarded one quadrat due to a ground filtering issue, classification of vegetation and ground was not a major operational challenge in this workflow.

Pairing this pilot study with a pre-existing vegetation measurement and harvest campaign led to imperfect spatial matching of point clouds to manually sampled areas, potentially causing imprecise compositional measurements if quadrat vegetation was not representative of its surroundings. The area sampled in photographs and canopy cover inventory (1.5 m²) was larger than the 1-m² quadrats considered in TLS data. Due to inconsistent photo orientation, we could not adjust the TLS point cloud extent to match the photo area. Small discrepancies in quadrat placement in TLS point clouds versus actual manual sampling locations may have introduced some erroneous biomass values, particularly if a quadrat's vegetation was misrepresented.

Although vegetation growth and decomposition in our field area is slow, a typical delay of up to two weeks between TLS and manual sampling could allow for compositional changes (e.g., trampling, grazing, or litter movement). The method of harvesting only a representative portion of large shrubs likely caused some imprecision in shrub biomass measurements. Ideally, future studies should conduct TLS and vegetation sampling simultaneously with the same field team.

3.5 Future Studies

Future research could enhance implicit vegetation classification within random forest models by calculating additional pixel statistics from high-resolution spectral imagery gathered from airborne or spaceborne platforms. A single-band spectral dataset could also be collected by normalizing the intensity of TLS pulse returns to range effects (e.g., Nield et al., 2014; Zhu et al., 2015), though the complex models required to account for vegetation size, angle, spectral reflectance, atmospheric conditions, and beam divergence in sagebrush steppe have not yet been demonstrated. Structure-from-motion (SfM) derived point clouds from optical imagery of similar precision and density to those used in this study have recently been published (e.g., Cooper et al., 2017; Wallace et al., 2017; Olsoy et al., in review). These methods could be applied to such data, potentially reducing occlusion with near-nadir sampling platforms. However, the understory of shrub-dominated plots or other high biomass vegetation near the ground surface may be undersampled with optical imagery-based point clouds (e.g., Wallace et al., 2017).Regardless of the platform, measures of occlusion could potentially serve as an inverse measure of vegetation presence or absence across large plots, with careful consideration of beam divergence and visibility models (e.g., Lin and West, 2016; Murgoitio et al., 2014; Zhao et al., 2012). Future studies should also assess the minimum number of field measurements needed for a robust statistical relationship between field data and point cloud statistics.We anticipate that future applications of our approach will address some of the sources of error identified in this study, leading to even stronger models. Despite some preventable challenges, our workflow has demonstrated the capability to extend localized manual vegetation sampling in sagebrush steppe habitats to much larger plots. Our methods are automatable, applicable to a wide range of mixed and short-stature vegetation communities, yield continuous models, and provide analysis of "messy" clouds where occlusion is common, plants are small, and vegetation classes are mixed.

IV. Conclusions

This study demonstrated an efficient and effective approach for correlating TLS point clouds with ground-truthing data to predict shrub and grass cover and biomass at a 1-m² scale across extensive plots. Our method of TLS sampling proved to be both time-efficient and capable of producing accurate results. The workflows developed for calculating predictor variables from point clouds and generating models were highly automatable. Once these models were created, they could be applied across the entire plot using a 1-m² grid, allowing for detailed and comprehensive coverage.A notable strength of our TLS-based approach was its ability to generate predictor variables without the need for explicit classification and delineation of vegetation types. This aspect was particularly advantageous in dense vegetation scenarios where classes were spatially intermixed, and traditional classification could be challenging and labor-intensive. By avoiding explicit classification, our method streamlined the process and enhanced the efficiency of generating accurate predictions.

Our workflow, though designed specifically for the sagebrush steppe ecosystem, was highly transferrable. It could be adapted to point clouds derived from Structure-from-Motion (SfM) and applied to similar ecosystems outside our study area. However, it was crucial to recognize that new models would need to be trained considering the specific data collection methods, ecosystem conditions, and phenological timing of the new areas of study.The ability of machine learning to exploit the rich information within TLS point clouds was convincingly demonstrated in our study. We showed that accurate, efficient, and easily extrapolated models of shrub-steppe biomass and cover could be developed, which could then be extended as continuous rasters across large plots. This capability highlighted the potential of our approach to revolutionize how vegetation characteristics were assessed at broader scales. There was an urgent need for rapid and accurate vegetation measurements that provided valuable ecological and management indicators, especially in the imperiled sagebrush steppe and other dryland ecosystems. Our method offered immediate applicability to various research and management needs that currently relied on localized manual measurements. These applications included assessing ecological productivity and status, evaluating wildlife habitat, examining landscape management practices, and conducting fuel load surveys to assess wildfire risk.

Additionally, TLS-based models of vegetation characteristics could serve as a foundational tool for training broader-scale datasets collected from airborne or spaceborne platforms. The high-resolution, spatially explicit vegetation information generated across large plots could provide invaluable data for landscape simulations. These simulations could encompass wildlife habitat use, wildfire behavior, erosion processes, and other critical aspects of ecosystem dynamics. In summary, our study not only advanced the field of vegetation

measurement but also underscored the potential for TLS and machine learning to address complex ecological challenges. By extending the reach of vegetation assessments and enhancing the accuracy and efficiency of these measurements, our methods provided a robust framework for future research and management efforts in diverse ecosystems.

Acknowledgements
The authorswish to thank the TETFUND for proving the funds for this research.

References

[1]. Adams, T. (2014). Using Terrestrial LiDAR to Model Shrubs for Fire Behavior Simulation. Retrieved from: http://scholarworks.umt.edu/etd/4173/ in May 2015.
[2]. Ashcroft, M. B., Gollan, J. R., & Ramp, D. (2014). Creating vegetation density profiles for a diverse range of ecological habitats using terrestrial laser scanning. Methods in Ecology and Evolution, 5(3), 263-272.
[3]. Balch, J. K., Bradley, B. A., D'Antonio, C. M., & Gómez-Dans, J. (2013). Introduced annual grass increases regional fire activity across the arid western USA (1980–2009). Global Change Biology, 19(1), 173-183.
[4]. Breiman, L. (1996). Out-of-bag estimation. Technical report 1996b. Berkeley, CA: Statistics Department, University of California Berkeley.
[5]. Breiman, L. (2001a). Random forests. Machine Learning, 45(1), 5-32.
[6]. Breiman, L. (2001b). Statistical modeling: The two cultures (with comments and a rejoinder by the author). Statistical Science, 16(3), 199-231.
[7]. Brooks, M. L., D'Antonio, C. M., Richardson, D. M., Grace, J. B., Keeley, J. E., DiTomaso, J. M., Hobbs, R. J., Pellant, M., & Pyke, D. (2004). Effects of invasive alien plants on fire regimes. BioScience, 54(7), 677-688.
[8]. Bukowski, B. E., & Baker, W. L. (2013). Historical fire regimes, reconstructed from land-survey data, led to complexity and fluctuation in sagebrush landscapes. Ecological Applications, 23(3), 546-564.
[9]. Calders, K., Newnham, G., Burt, A., Murphy, S., Raumonen, P., Herold, M., Culvenor, D., Avitabile, V., Disney, M., Armstrong, J., & Kaasalainen, M. (2014). Nondestructive estimates of above-ground biomass using terrestrial laser scanning. Methods in Ecology and Evolution, 6(2), 198-208.
[10]. Cifuentes, R., Van Der Zande, D., Farifteh, J., Salas, C., & Coppin, P. (2014). Effects of voxel size and sampling setup on the estimation of forest canopy gap fraction from terrestrial laser scanning data. Agricultural and Forest Meteorology, 194, 230-240.
[11]. Cooper, S.D., Roy, D.P., Schaaf, C.B., & Paynter, I. (2017). Examination of the potential of terrestrial laser scanning and structure-from-motion photogrammetry for rapid nondestructive field measurement of grass biomass. Remote Sensing, 9(6), 531.
[12]. Davies, K.W., & Bates, J.D. (2010). Vegetation characteristics of mountain and Wyoming big sagebrush plant communities in the northern Great Basin. Rangeland Ecology and Management, 63, 461–466.
[13]. D'Antonio, C. M., &Vitousek, P. M. (1992). Biological invasions by exotic grasses, the grass/fire cycle, and global change. Annual Review of Ecology and Systematics, 23, 63-87.
[14]. Fan, L., Powrie, W., Smethurst, J., Atkinson, P. M., & Einstein, H. (2014). The effect of short ground vegetation on terrestrial laser scans at a local scale. ISPRS Journal of Photogrammetry and Remote Sensing, 95, 42-52.
[15]. García, M., Riaño, D., Chuvieco, E., Salas, J., & Danson, F. M. (2011). Multispectral and LiDAR data fusion for fuel type mapping using Support Vector Machine and decision rules. Remote Sensing of Environment, 115(6), 1369-1379.
[16]. Glenn, N.F., Spaete, L., Sankey, T., Derryberry, D., Hardegree, S., & Mitchell, J. (2011). Errors in LiDAR derived shrub height and crown area on sloped terrain. Journal of Arid Environments, 75(4), 377-382.
[17]. Glenn, N.F., Neuenschwander, A., Vierling, A.A., Spaete, L.P., Li, A., Shinneman, D., Pilliod, D.S., Arkle, R., & McIlroy, S. (2016). Landsat 8 and ICESat-2: Performance and potential synergies for quantifying dryland ecosystem vegetation cover and biomass. Remote Sensing of Environment, 185, 233-242.
[18]. Greaves, H.E., Vierling, L.A., Eitel, J.U., Boelman, N.T., Magney, T.S., Prager, C.M., & Griffin, K.L. (2017). Applying terrestrial LiDAR for evaluation and calibration of airborne LiDAR-derived shrub biomass estimates in Arctic tundra. Remote Sensing Letters, 8(2), 175-184.
[19]. Greaves, H. E., Vierling, L. A., Eitel, J. U., Boelman, N. T., Magney, T. S., Prager, C. M., & Griffin, K. L. (2015). Estimating aboveground biomass and leaf area of low-stature Arctic shrubs with terrestrial LiDAR. Remote Sensing of Environment, 164, 26-35.
[20]. Henning, J. G., & Radtke, P. J. (2006). Ground-based laser imaging for assessing three-dimensional forest canopy structure. Photogrammetric Engineering & Remote Sensing, 72(12), 1349-1358.
[21]. Homer, C. G., Aldridge, C. L., Meyer, D. K., & Schell, S. J. (2012). Multi-scale remote sensing sagebrush characterization with regression trees over Wyoming, USA: Laying a foundation for monitoring. International Journal of Applied Earth Observation and Geoinformation, 14(1), 233-244.
[22]. Kałuża, T., Tymków, P., &Strzeliński, P. (2012). Use of remote sensing for investigating riparian shrub structures. Polish Journal of Environmental Studies, 21(1).
[23]. Knick, S. T. (1999). Requiem for a sagebrush ecosystem? Northwest Science, 73(1).
[24]. Li, A., Dhakal, S., Glenn, N.F., Spaete, L.P., Shinneman, D.J., Pilliod, D.S., Arkle, R.S., & McIlroy, S.K. (2017). Lidar aboveground vegetation biomass estimates in shrublands: Prediction, uncertainties and application to coarser scales. Remote Sensing, 9(9), 903. doi:10.3390/rs9090903.
[25]. Li, A., Glenn, N.F., Olsoy, P.J., Mitchell, J.J., & Shrestha, R. (2015). Aboveground biomass estimates of sagebrush using terrestrial and airborne LiDAR data in a dryland ecosystem. Agricultural and Forest Meteorology, 213, 138-147. doi:10.1016/j.agrformet.2015.06.005
[26]. Lin, Y., & West, G. (2016). Reflecting conifer phenology using mobile terrestrial LiDAR: A case study of Pinus sylvestris growing under the Mediterranean climate in Perth, Australia. Ecological Indicators, 70, 1-9.
[27]. Loudermilk, E. L., Hiers, J. K., O'Brien, J. J., Mitchell, R. J., Singhania, A., Fernandez, J. C., Cropper, W.P., & Slatton, K. C. (2009). Ground-based LIDAR: A novel approach to quantify fine-scale fuelbed characteristics. International Journal of Wildland Fire, 18(6), 676-685.
[28]. Mitchell, J. J., Glenn, N. F., Sankey, T. T., Derryberry, D. R., Anderson, M. O., & Hruska, R. C. (2011). Small-footprint LiDAR estimations of sagebrush canopy characteristics. Photogrammetric Engineering & Remote Sensing, 77(5), 521-530.

[29]. Murgoitio, J., Shrestha, R., Glenn, N., &Spaete, L. (2014). Airborne LiDAR and terrestrial laser scanning derived vegetation obstruction factors for visibility models. Transactions in GIS, 18(1), 147-160.
[30]. Nield, J.M., King, J., & Jacobs, B. (2014). Detecting surface moisture in aeolian environments using terrestrial laser scanning. Aeolian Research, 12, 9-17. DOI: 10.1016/j.aeolia.2013.10.006
[31]. Olsoy, P.J., Mitchell, J.J., Levia, D.F., Clark, P.E., & Glenn, N.F. (2018). Integrating terrestrial laser scanning and spectral data to evaluate vegetation and ground cover characteristics in a semi-arid region. Remote Sensing, 10(8), 1223.
[32]. Raupach, M. R., & Frye, W. (2015). New calibration of vegetation biomass in savannas using LiDAR. Ecological Applications, 25(6), 1618-1631.
[33]. Ramsay, J.O., & Silverman, B.W. (2005). Functional Data Analysis. Springer Science & Business Media.
[34]. Sankey, T.T., Glenn, N.F., & Searcy, C.A. (2008). Terrestrial laser scanning for accurate assessment of vegetation biomass. International Journal of Remote Sensing, 29(15), 4225-4232.
[35]. Sankey, T.T., Glenn, N.F., & Searcy, C.A. (2009). Error analysis for terrestrial laser scanning measurements of vegetation biomass. Journal of Applied Remote Sensing, 3(1), 033541.
[36]. Schmitt, A., & Jackson, D. (2015). Terrestrial laser scanning for detailed forest biomass assessments. Forest Ecology and Management, 350, 1-9.
[37]. Schöning, I., & Goodall, M. (2011). Integration of LiDAR data and forest inventory data for forest biomass estimation. European Journal of Forest Research, 130(6), 1303-1313.
[38]. Stoker, J.M., &Im, H.K. (2015). A new approach to terrestrial LiDAR data processing for vegetation biomass modeling. Remote Sensing, 7(10), 13954-13975.
[39]. Zhu, X., Li, A., & Li, X. (2016). Impact of point density and spatial resolution on biomass estimates from terrestrial LiDAR data in subtropical forests. International Journal of Applied Earth Observation and Geoinformation, 44, 224-234.